agronomy

MDPI

Article

Metabolic Profiling and Transcriptome Analysis Provide Insights into the Anthocyanin Types and Biosynthesis in *Zingiber striolatum* Diels Flower Buds in Three Planting Modes

Dan Zhou [1], Tianhong Wang [1], Qian Zhao [2,3] and Guofei Tan [2,3,*]

[1] Zunyi Academy of Agricultural Sciences, Zunyi 563000, China; 18404968223@163.com (D.Z.); tianhong9843@163.com (T.W.)
[2] Institute of Horticultural, Guizhou Academy of Agricultural Science/Guizhou Horticultural Engineering Technology Research Centers/Ministry of Agriculture and Rural Affairs Key Laboratory of Crop Genetic Resources and Germplasm Innovation in Karst Region, Guiyang 550006, China; zhaoqian@mails.jlau.edu.cn
[3] Faculty of Agronomy, Jilin Agricultural University, Changchun 130118, China
* Correspondence: tgfei@foxmail.com

Abstract: The flower buds of *Zingiber striolatum* Diels are considered a special vegetable in China, and they are rich in anthocyanins. However, the detailed composition types and the molecular mechanism of anthocyanin biosynthesis in *Z. striolatum* flower buds are still unclear. In this study, targeted metabolites were used to analyze and identify the anthocyanin types of *Z. striolatum* in three planting modes: monoculture (CK), intercropping with maize (ZP), and intercropping with soybean (SP). A total of 48 anthocyanins were identified with significant differential accumulation in *Z. striolatum* flower buds. Among them, cyanidin-3-*O*-glucoside was the main composition type of anthocyanins. Furthermore, the composition types of blue anthocyanin were identified in flower buds. A total of 15 structure genes were obtained from the transcriptome database of *Z. striolatum* flower buds. The qRT-PCR results revealed that the expression levels of *ZsC4H-1*, *ZsC4H-2*, *ZsCHS-2*, *ZsCHI*, *ZsF3H*, *ZsF3′H*, *ZsDFR*, *ZsF3′5′H-3*, and *ZsANS* genes were the highest in the ZP model. This study showed that the ZP model contributes to anthocyanin synthesis and accumulation of *Z. striolatum* flower buds among the three planting modes of *Z. striolatum*. These findings provide valuable information for research on the planting model and anthocyanin biosynthesis in *Z. striolatum* flower buds.

Keywords: *Z. striolatum*; flower buds; metabolite profiling; transcriptome; anthocyanins

Citation: Zhou, D.; Wang, T.; Zhao, Q.; Tan, G. Metabolic Profiling and Transcriptome Analysis Provide Insights into the Anthocyanin Types and Biosynthesis in *Zingiber striolatum* Diels Flower Buds in Three Planting Modes. *Agronomy* **2024**, *14*, 1414. https://doi.org/10.3390/agronomy14071414

Academic Editor: Moshe Reuveni

Received: 18 May 2024
Revised: 18 June 2024
Accepted: 24 June 2024
Published: 28 June 2024

1. Introduction

Zingiber striolatum Diels, belonging to the Ginger family, is an herbaceous perennial root plant that has been cultivated nationwide in China in regions such as Guizhou, Yuannan, and Jiangsu [1,2]. The flower buds of *Z. striolatum* are considered a unique vegetable in China and are rich in anthocyanins [3]. The *Z. striolatum* roots are also used in traditional Chinese medicine for the treatment of constipation and diabetes and pain relief and detoxification [4–7].

Anthocyanins are important secondary metabolites that are widely distributed in many plants, such as tomato, onion, cabbage, purple carrot, blood orange, and red-flesh apple [8,9]. Anthocyanins protect plants from damage caused by high light irradiation, high temperature, low temperature, pathogens, and free radical scavengers produced in cells [10–12]. In higher plants, anthocyanins play crucial roles in flower color and attracting insects for pollination [13,14]. Anthocyanins are important nutrients and medicines for human health [15–17]. Furthermore, anthocyanins can be used as selection markers for breeding and biological research [18,19]. In the plant kingdom, anthocyanins are synthesized from phenylalanine through a biosynthetic pathway [20]. Anthocyanin biosynthesis

can be divided into three main phases. The first step, which is the phenylpropanoid pathway, involves the conversion of phenylalanine to cinnamic acid to coumaric acid to 4-coumaroyl CoA, and these reactions are catalyzed by phenylalanine ammonia-lyase (PAL), cinnamate-4-hydroxylase (C4H), and 4-coumaroyl CoA ligase (4CL), respectively [20–22]. The second step, which is the flavonoid pathway, involves the conversion of 4-coumaroyl CoA to chalcone and naringein to dihydroflavonol, and these reactions are catalyzed by chalcone synthase (CHS), chalcone isomerase (CHI), and flavanone 3-hydroxylase (F3H), respectively [19–23]. The final step, which is the anthocyanin pathway, involves the conversion of dihydroflavonols to leucoanthocyanidins to anthocyanidins and the further modification of anthocyanidins; these reactions are catalyzed by dihydroflavonol reductase (DFR), anthocyanidin synthase (ANS, also called leucoanthocyanidin dioxygenase), and cyanidin 3-*O*-galactosyltransferase (3GT) [21–23]. The biosynthetic pathway for anthocyanins was first identified from *Arabidospis thaliana* leaf tissues in 2002 [24]. This biosynthesis pathway has been studied in numerous plant species, such as carrot [25], *A. thaliana* [26], sweet cherry [27], blood-flesh peach [28], and herbaceous peony [29].

The anthocyanins are divided into six categories in plants: petunidin, delphinidin, malvidin, peonidin, cyanidin, and pelargonidin [30]. The difference in anthocyanin type and content leads to the different color patterns in plants, such as fruit skins, fleshes, leaves, and so on [8,9]. In the flowers of *Pericallis hybrida*, the cultivars with pink flowers mainly accumulate pelargonidin, the cultivars with red flowers mainly contain cyanidin, and the cultivars with blue flowers mainly comprise delphinidin [13,31]. Chai et al. collected and analyzed the type and content of anthocyanins in 74 blueberry varieties and showed that peonidin-3-glucoside mainly had anthocyanin content in blueberry fruit, but the content of monomeric compounds was different among blueberry varieties [32]. At the same time, the anthocyanin synthesis was also affected by gene regulation, such as *Viola tricolor VtF3′5′H* and *Iris tectorum ItDFR* genes, which were overexpressed, and the expression of endogenous *RcDFR* gene was inhibited in *R. chinensis*, leading to the production of blue–purple varieties of *R. chinensis* [33]. Similarly, blue chrysanthemum varieties with high delphinidin content have been obtained by introducing the *CmF3′5′H* gene of *Campanula medium* and the *CtUA3′5′GT* gene of *Clitoria ternatea* into chrysanthemum [34].

Z. striolatum is a shady crop plant that likes to live in a cool environment. In a monoculture, direct sunlight can affect its growth and development. In recent years, intercropping with maize or soybeans has provided a cool environment for the growth of *Z. striolatum*, improving the yield of *Z. striolatum* flower buds and the content of anthocyanins in the Qixingguan District of Bijie City, China. To date, no insights have been made available on anthocyanin biosynthesis in *Z. striolatum*. In this study, we performed metabolite profiling and transcriptome analysis to explore the composition types, content, and molecular mechanism of anthocyanin biosynthesis in the flower buds of *Z. striolatum* among three cropping modes (monoculture (CK), intercropping with maize (ZP), and intercropping with soybean (SP)). The targeted metabolites were used to analyze and identify the anthocyanin types, and the expression levels of structural genes in anthocyanin biosynthesis in *Z. striolatum* were verified by the quantitative real-time polymerase chain reaction (qRT-PCR).

2. Materials and Methods

2.1. Plant Material and Sampling

Qixingguan District of Bijie City (27.622° N, 105.411° E, altitude 1320.600 m), the largest cultivated area of *Z. striolatum* in Guizhou Province was selected to adopt three planting modes, namely *Z. striolatum* monoculture (CK), intercropping with maize (ZP), and intercropping with soybean (SP), each planting pattern was repeated 3 times, 5 hectares each repeat. The spacing was 120 cm × 80 cm, with about 20,000~21,000 maize plants per hectare in ZP. The spacing was 120 cm × 20 cm, about 80,000~84,000 soybean plants per hectare in SP. Maize and soybeans were planted directly on 3 May 2023. *Z. striolatum* flower buds were harvested on 29 July 2023 (8:00 AM–9:00 AM) and sampled during the commodity period. Three biological replicates were set for each sample, and 20 flower buds were taken

for each repetition, repeated 3 times. After harvesting, water was used to clean the dirt of *Z. striolatum* flower buds. Portions of the samples were vacuum freeze-dried for targeted metabolomics analysis. Some were immediately frozen in liquid nitrogen and then stored at −80 °C for RNA extraction and determination of total anthocyanins content.

2.2. Targeted Metabolite Profiling Analysis

The sample was freeze-dried and ground into powder (30 Hz, 1.5 min) using a ball mill (MM400, Retsch, Retsch-Allee, Germany) and stored at −80 °C. 0.05 mg powder was weighed and extracted with 0.5 mL methanol/water/hydrochloric acid (500:500:1, *v*/*v*/*v*). Then, the extract was vortexed for 5 min, subjected to ultrasound for 5 min, and centrifuged at 12,000 rpm at 4 °C for 3 min (5424R, Eppendorf, Hamburg, Germany). The residue was re-extracted by repeating the above-mentioned steps under the same conditions. The supernatants were collected and filtrated through a hydrophilic nylon membrane filter with a pore size of 0.22 μm before LC-MS/MS analysis (Q-Trap 6500$^+$, SCIEX, Framingham, MA, USA).

UPLC conditions: The sample extracts were analyzed using a UPLC-ESI-MS/MS system (UPLC, ExionLC™ AD, https://sciex.com.cn/ (accessed on15 February 2024); MS, Applied Biosystems 6500 Triple Quadrupole, https://sciex.com.cn/ (accessed on 15 February 2024)). The analytical conditions were as follows: UPLC: column, Waters ACQUITY BEH C18 (1.7 μm, 2.1 mm × 100^{-1} mm); solvent system A, water (0.1% formic acid, Sigma-Aldrich, Waltham, MA, USA): solvent system B, methanol (0.1% formic acid); gradient program, 95:5 *v*/*v* at 0 min, 50:50 *v*/*v* at 6 min, 5:95 *v*/*v* at 12 min, hold for 2 min, 95:5 *v*/*v* at 14 min, hold for 2 min; flow rate, 0.35 mL·min^{-1}; temperature, 40 °C; injection volume, 2 μL.

The mass spectrometry conditions mainly include: The temperature of the electrospray ionization (ESI) source was 550 °C, the mass spectrum voltage in positive ion mode was 5500 V, and the Curtain Gas (CUR) was 35 psi. In Q-Trap 6500$^+$, each ion pair is scanned and detected based on optimized declustering potential (DP) and collision energy (CE).

2.3. Qualitative and Quantitative Analysis of Metabolites

Based on the standard substance, the MWDB database (Metware Database) was constructed to qualitatively analyze the mass spectrometry data. Anthocyanin was analyzed using scheduled multiple reaction monitoring (MRM). First, the precursor ions of the target substance were screened by the four-stage bar, and the corresponding ions of other molecular weight substances were preliminarily excluded. The precursor ions were ionized by the collision chamber to form multiple fragment ions, and the fragment ions were triple-filtered to select the required characteristic fragment ions to eliminate the interference of non-target ions. After obtaining the mass spectrometry data of different samples, the chromatographic peaks of all targets were integrated and quantitatively analyzed using a standard curve. Data acquisitions were performed using Analyst 1.6.3 software (Sciex). Multiquant 3.0.3 software (Sciex) was used to quantify all metabolites.

2.4. Data Processing and Evaluation

Data preprocessing: The mass spectrum data were processed using the Analyst 1.6.3 software. MultiQuant 3.0.3 software was used to process the mass spectrum data, reference the retention time and peak type information of the standards, and the chromatographic peaks detected in different samples were corrected integrally to ensure the accuracy of qualitative and quantitative analysis.

Standard curve: To prepare a standard solution of 0.01, 0.05, 0.1, 0.5, 1.0, 5.0, 10, 50, 100, 500, 1000, 2000, and 5000 ng·mL^{-1} for anthocyanins analysis, the peak intensity data of the corresponding quantitative signals were obtained, and the standard curves of different substances were drawn with the reference concentration as the horizontal coordinate and the peak area as the vertical coordinate.

Calculation of anthocyanin content: The integral peak area of all the samples was put into the linear equation of the standard curve and then put into the calculation formula. Contents of metabolites in the sample ($\mu g \cdot g^{-1}$) = C × V × 1,000,000 m^{-1}. C: Concentration value ($ng \cdot mL^{-1}$) of the area of the integral peak in the sample substituted for the standard curve; V: volume (mL) of the solution used at the time of extraction; m: the sample quality (g). The coefficient of variation was conducted using the Empirical Cumulative Distribution Function (ECDF, https://www.mathworks.com/help/stats/ecdf.html (accessed on 20 February 2024)).

2.5. Total Anthocyanin Content Determination

The total anthocyanin content of flower buds was determined in accordance with Xu et al. method [25]. The determination of total anthocyanin content in *Z. striolatum* flower buds among three planting modes was conducted as previously described. Fresh samples of *Z. striolatum* flower buds were ground into powder using liquid nitrogen. Not less than 2 g powder was weighed and placed into test tubes, added with 20 mL 0.1% methanol, and extracted for 8 h in dark conditions at room temperature. Three biological replicates were set for each sample. The extract was filtered using a 0.25 μm filter, and total anthocyanin quantities were reported in mg cyanidin 3-*O*-galactoside equivalents per g FW ($mg \cdot g^{-1}$ g, FW). Values were the means of three independent experiments.

2.6. Transcriptome Analysis and Genes Identification

According to the metabolic pathway for anthocyanins, anthocyanin-related gene sequences were obtained for the transcriptome database of *Z. striolatum* constructed by our group. The open reading frame and the amino acid sequence of these genes were obtained using BioXM2.7.1 software. Then, the amino acid sequences were compared with that of *Zingiber officinale* using the NCBI database (BioSample: SAMN15647981) to predict the correctness and integrity of the gene sequences. Finally, the gene sequence information of *Z. striolatum* involved in the anthocyanidin biosynthesis is listed in Table S1.

2.7. RNA Extraction and Quantitative RT-PCR (qRT-PCR)

The total RNA of flower bud samples (harvested between 8:00 AM and 9:00 AM, 29 July 2023) at three cropping patterns was isolated using TaKaRa MiniBEST Plant RNA Extraction Kit. One microgram of total RNA was used for reverse transcription into cDNA using the First Strand cDNA Synthesis Kit (Nuode Biotech., Beijing, China). qRT-PCR primers for these genes encoding the key enzymes associated with the anthocyanin biosynthesis are listed in Table S2. qRT-PCR was conducted using SYBR Premix *Ex* Tag (TaKaRa, San Jose, CA, USA) and cDNA as the template. Results were analyzed using the $2^{-\Delta\Delta CT}$ method with *ZsActin* gene expression level as an internal reference. The *ZsActin* gene is a gene that is stably expressed during flower development based on our study (Unpublished). Three biological and three technical replicates were set in this study.

2.8. Statistical Analysis

Significant analysis was calculated using ANOVA (Analysis of variance), and Pearson's correlation was used for correlation analysis of the anthocyanin content and expression levels of anthocyanin-synthesis-related genes. Microsoft Excel 2007 and Origin 2021 software were used for data processing and mapping, respectively.

3. Results

3.1. Flower Buds of Z. striolatum in Three Planting Modes

Three main planting modes of *Z. striolatum* in Guizhou Province were considered, namely *Z. striolatum* monoculture (CK) (Figure 1(A1)), intercropping with maize (ZP) (Figure 1(B1)), and intercropping with soybean (SP) (Figure 1(C1)). In the three planting modes, the commodity organs and quality of *Z. striolatum* were significantly different. In CK, few flower buds were found in the roots (Figure 1(A2)), and the number of flower buds

in a single plant was 7.87, and the commodity flower buds were small (single flower bud weight was 25.12 g, and the flower bud size was only 4.51 cm × 2.11 cm, Table 1), and had obvious chlorophyll accumulation at the top of *Z. striolatum* flower buds (Figure 1(A3)). The *Z. striolatum* roots produced abundant flower buds (Figure 1(B2)), the number of flower buds in single plant was 11.62, and the commodity flower buds were large (single flower bud weight was 35.08 g, and the flower bud size was only 4.51 cm × 2.69 cm, Table 1), and the anthocyanins was accumulation obvious (Figure 1(B3)) in ZP (0.26 $mg \cdot g^{-1}$, FW, Table 1). The number of root flower buds of SP was less than that of ZP and higher than that of CK (Figure 1(C2)), and the commodity flower buds were medium, but the anthocyanin was significantly lower than that of CK and ZP (Figure 1(C3), Table 1). The highest yield of flower buds in ZP was 1384.13 $kg \cdot 667\ m^{-2}$, the flower buds medium yield was 1179.22 $kg/667\ m^2$ in SP, the lowest flower buds was 1094.66 $kg/667\ m^2$ in the CK (Table 1).

Figure 1. The field, root flower buds, and commodity flower buds of *Z. striolatum* under three planting modes. (**A1**): CK; (**B1**): ZP; (**C1**): SP; (**A2**): Root flower buds of CK; (**B2**): Root flower buds of ZP; (**C2**): Root flower buds of SP; (**A3**): Commodity flower buds of CK; (**B3**): Commodity flower buds of ZP; (**C3**): Commodity flower buds of SP.

Table 1. The information on *Z. striolatum* flower buds among three planting modes.

No	The Number of Flower Buds in Single Plant	Single Flower Bud Weight (g)	The Flower Buds Size (Length × Width, cm)	Anthocyanidin Content ($mg \cdot g^{-1}$, FW)	Yield ($kg/667\ m^2$)
CK	7.87 ± 1.99 c	25.12 ± 3.15 c	4.51 × 2.11 b	0.16 ± 0.04 b	1094.66 ± 32.67 b
ZP	11.62 ± 2.78 a	35.08 ± 3.23 a	6.12 × 2.69 a	0.26 ± 0.06 a	1384.13 ± 41.45 a
SP	9.08 ± 2.57 b	28.33 ± 2.18 b	5.23 × 2.34 b	0.09 ± 0.03 c	1179.22 ± 35.78 b

Different lowercase letters indicate the significance of the difference in this table ($p < 0.05$).

3.2. Types and Total Anthocyanin Content in Flower Buds among Three Planting Modes

To explore the types of anthocyanins in the *Z. striolatum* flower buds, 48 anthocyanins were identified from *Z. striolatum* flower buds by targeted metabolomics. They were divided into 6 categories (Table 2). Among them, there were 5 petunidin, 9 delphinidin, 6 malvidin, 7 peonidin, 17 cyanidin, and 4 pelargonidin. The metabolomics analysis results showed that the anthocyanins components in the *Z. striolatum* flower buds were complex and diverse. Furthermore, anthocyanin composition types of blue anthocyanins were also identified in flower buds, such as 9 delphinidin types, 5 petunidin types, and 6 malvidin types.

Table 2. The anthocyanin types and content of *Z. striolatum* flower buds among three planting modes. Anthocyanin quantities were reported in μg cyanidin 3-*O*-galactoside equivalents per g DW (μg·g^{-1} g, DW).

No	Compounds	Formula	RT (min)	Molecular Weigh	CK (μg·g^{-1}, DW)	ZP (μg·g^{-1}, DW)	SP (μg·g^{-1}, DW)	Type
1	Petunidin-3-*O*-(6-*O*-p-coumaroyl)-glucoside	C31H29O14	11.95	625.156	0.0175	0.0172	0.0178	Petunidin
2	Petunidin-3-*O*-(6-*O*-malonyl-beta-D-glucoside)	C25H25O15	12.16	565.119	0.0055	0.0072	0.0039	
3	Petunidin-3-O-5-O-(6-O-coumaroyl)-diglucoside	C37H39O19	9.62	787.209	0.0026	0.0028	0.0025	
4	Petunidin-3-*O*-glucoside	C22H23O12	8.23	479.119	6.7087	11.6088	1.8086	
5	Petunidin-3-*O*-rutinoside	C28H33O16	8.76	625.177	8.2097	13.0901	3.3293	
6	Delphinidin-3-*O*-(6-*O*-malonyl-beta-D-glucoside)	C24H23O15	11.08	551.104	0.0028	0.0000	0.0056	Delphinidin
7	Delphinidin-3-*O*-(6-*O*-malonyl)-glucoside-3′-glucoside	C30H33O20	11.14	713.157	0.0050	0.0000	0.0100	
8	Delphinidin-3-*O*-(6″-*O*-coumaroyl)rhamnoside-5-O-glucoside	C36H37O18	9.80	757.198	0.0196	0.0234	0.0158	
9	Delphinidin-3-*O*-(6″-*O*-tartaryl) glucoside	C25H25O17	10.02	597.109	0.0040	0.0081	0.0000	
10	Delphinidin-3-*O*-(coumaroyl) glucoside-5-*O*-galactoside	C36H37O19	8.06	773.193	0.0168	0.0181	0.0155	
11	Delphinidin-3-*O*-sophoroside	C27H31O17	6.08	627.156	0.0268	0.0438	0.0097	
12	Delphinidin-3-*O*-glucoside	C21H21O12	6.59	465.103	29.0060	48.4435	9.5686	
13	Delphinidin-3-*O*-rutinoside	C27H31O16	7.18	611.161	19.0167	29.9917	8.0418	
14	Delphinidin-caffeoyl-rutinoside	C36H37O19	5.55	773.193	0.0140	0.0281	0.0000	
15	Malvidin-3-*O*-(6″-*O*-acetyl) galactoside	C25H27O13	10.12	535.145	0.0079	0.0157	0.0000	Malvidin
16	Malvidin-3-*O*-(6″-*O*-acetyl) glucoside	C25H27O13	11.70	535.145	0.0120	0.0079	0.0160	

Table 2. *Cont.*

No	Compounds	Formula	RT (min)	Molecular Weigh	CK (μg·g^{-1}, DW)	ZP (μg·g^{-1}, DW)	SP (μg·g^{-1}, DW)	Type
17	Malvidin-3-*O*-(glucosyl) glucuronide	C29H33O18	9.92	669.167	0.0497	0.0774	0.0220	Malvidin
18	Malvidin-3-*O*-arabinoside	C22H23O11	9.96	463.124	0.2362	0.4005	0.0718	
19	Malvidin-3-*O*-glucoside	C23H25O12	9.50	495.135	5.1609	9.3082	1.0136	
20	Malvidin-3-*O*-rhamnoside	C23H25O11	10.67	477.140	0.0049	0.0000	0.0097	
21	Peonidin-3,5-*O*-diglucoside	C28H33O16	6.88	625.177	0.0367	0.0734	0.0000	Peonidin
22	Peonidin-3-*O*-(6″-*O*-acetyl-malonyl) glucoside	C27H27O15	4.36	591.135	0.0008	0.0016	0.0000	
23	Peonidin-3-*O*-arabinoside	C21H21O10	9.55	433.113	0.3435	0.6870	0.0000	
24	Peonidin-3-*O*-glucoside	C22H23O11	9.14	463.124	38.4653	71.1945	5.7360	
25	Peonidin-3-*O*-sambubioside	C27H31O15	9.18	595.166	6.6964	12.5555	0.8373	
26	Peonidin-3-*O*-sambubioside-5-*O*-glucoside	C33H41O20	6.91	757.219	0.0104	0.0208	0.0000	
27	Peonidin-hydroxyben-malonyl-glucoside-xyloside	C37H37O20	9.80	801.188	0.0020	0.0039	0.0000	
28	Cyanidin-3-*O*-(6-*O*-p-coumaroyl)-glucoside	C30H27O13	12.34	595.145	0.7768	0.8236	0.7301	Cyanidin
29	Cyanidin-3,5-*O*-diglucoside	C27H31O16	5.56	611.161	0.0593	0.1185	0.0000	
30	Cyanidin-3-*O*-(6″-*O*-ferulyl-xylosyl) glucoside	C36H37O18	9.16	757.198	0.0062	0.0073	0.0052	
31	Cyanidin-3-*O*-(6-*O*-malonyl-beta-D-glucoside)	C24H23O14	10.38	535.109	0.8690	1.5534	0.1846	
32	Cyanidin-3-*O*-(6″-*O*-acetyl-2″-*O*-xylosyl) glucoside	C28H31O16	8.79	623.161	0.0043	0.0086	0.0000	
33	Cyanidin-3-*O*-(6″-*O*-coumaryl) galactoside	C30H27O13	11.72	595.145	0.2080	0.2524	0.1635	
34	Cyanidin-3-*O*-(tartaryl)rhamnoside-5-*O*-glucoside	C31H35O20	8.23	727.172	0.0092	0.0184	0.0000	
35	Cyanidin-3-[6″-(rhamnosyl) glucoside]	C27H31O15	7.24	595.166	0.2542	0.4179	0.0906	
36	Cyanidin-3-[6″-(acetyl)xylosyl]-xyloside	C27H29O15	8.75	593.151	0.1188	0.2198	0.0179	
37	Cyanidin-3-*O*-arabinoside	C20H19O10	8.04	419.098	0.6138	1.1575	0.0702	

Table 2. *Cont.*

No	Compounds	Formula	RT (min)	Molecular Weigh	CK (μg·g^{-1}, DW)	ZP (μg·g^{-1}, DW)	SP (μg·g^{-1}, DW)	Type
38	Cyanidin-3-*O*-sophoroside	C27H31O16	7.03	611.161	1.9012	3.4138	0.3886	Cyanidin
39	Cyanidin-3-gentiobioside	C27H31O16	6.50	611.161	0.0140	0.0244	0.0036	
40	Cyanidin-3-*O*-xyloside	C20H19O10	9.81	419.098	0.7835	1.4511	0.1159	
41	Cyanidin-3-*O*-glucoside	C21H21O11	7.60	449.109	641.2958	1091.5414	191.0501	
42	Cyanidin-3-*O*-sambubioside	C26H29O15	7.71	581.151	1.9455	3.5407	0.3502	
43	Cyanidin-3-*O*-rhamnoside	C21H21O10	10.76	433.113	0.0018	0.0000	0.0036	
44	Cyanidin-rutinoside-rhamnoside	C33H41O19	11.12	741.224	0.0009	0.0000	0.0018	
45	Pelargonidin-3-*O*-(6″-*O*-acetyl) galactoside	C23H23O11	10.26	475.124	0.0035	0.0000	0.0071	Pelargonidin
46	Pelargonidin-3-*O*-galactoside	C21H21O10	7.86	433.113	0.0047	0.0000	0.0093	
47	Pelargonidin-3-*O*-glucoside	C21H21O10	8.55	433.113	5.9417	10.7787	1.1047	
48	Pelargonidin-3-*O*-sambubioside	C26H29O14	8.66	565.156	0.0048	0.0095	0.0000	

The content of anthocyanin components was determined in three planting modes by targeted metabolomics. The results revealed that 48 anthocyanin components were detected in CK, 7 anthocyanin components (delphinidin-3-*O*-(6-*O*-malonyl-beta-D-glucoside),delphinidin-3-*O*-(6-*O*-malonyl)-glucoside-3′-glucoside, malvidin-3-*O*-rhamnoside, cyanidin-3-*O*-rhamnoside, cyanidin-rutinoside-rhamnoside, pelargonidin-3-*O*-(6″-*O*-acetyl)galactoside, pelargonidin-3-*O*-galactoside) were detected in ZP, and 12 anthocyanin components (delphinidin-3-*O*-(6″-*O*-tartaryl)glucoside, delphinidin-caffeoyl-rutinoside, malvidin-3-*O*-(6″-*O*-acetyl)galactoside, peonidin-3,5-*O*-diglucoside, peonidin-3-*O*-(6″*O*-acetyl-malonyl)glucoside, peonidin-3-*O*-arabinoside, peonidin-3-*O*-sambubioside-5-*O*-glucoside, peonidin-hydroxyben-malonyl-glucoside-xyloside, cyanidin-3,5-*O*-diglucoside, cyanidin-3-*O*-(6″-*O*-acetyl-2″-*O*-xylosyl)glucoside, cyanidin-3-*O*-(tartaryl)rhamnoside-5-*O*-glucoside, pelargonidin-3-*O*-sambubioside) were detected in SP.

Among the three planting modes, the anthocyanin content was the highest (1312.9663 μg g^{-1}, DW) in ZP, followed by CK (768.8993 μg g^{-1}, DW), and the anthocyanin content was the lowest (224.8324 μg g^{-1}, DW) in SP (Table 2). At the same time, cyanidin-3-*O*-glucoside content was the highest among all kinds of anthocyanin in the three planting modes. The content of total anthocyanin and cyanidin-3-*O*-glucoside were analyzed in the three planting modes, and the results indicated that the total anthocyanin content was consistent with the changing trend of cyanidin-3-*O*-glucoside in the three planting modes (Figure 2). In general, the planting mode of ZP was conducive to the accumulation of anthocyanin, and cyanidin-3-*O*-glucoside was the main anthocyanin component in the *Z. striolatum* flower buds.

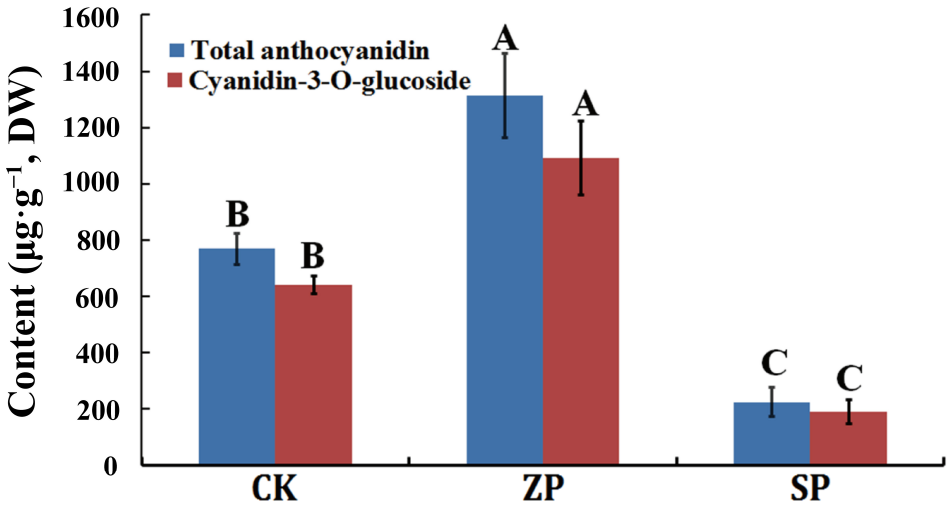

Figure 2. The content of total anthocyanin and cyanidin-3-*O*-glucoside. The capitalized A, B, and C indicated a significant difference ($p < 0.01$) in this figure.

3.3. Transcriptome Analysis and Gene Identification

We obtained 15 anthocyanin-related structure genes from the transcriptome database of *Z. striolatum*, which were 1 *ZsPAL*, 2 *ZsC4H*, 2 *ZsCHS*, 1 *ZsCHI*, 4 *ZsF3′5′H*, 1 *ZsF3′H*, 1 *ZsF3′H*, 1 *ZsDFR*, 1 *ZsANS*, and 1 *Zs3GT* (Figure 3). The retrieved genes were deduced into corresponding amino acid sequences, and the amino acid sequences were compared with those of the *Z. officinale* plant using the NCBI online website. The results showed that the obtained anthocyanin-related gene sequences were complete, the consistency of gene sequences with *Z. officinale* plant was high, and the consistency level was between 88% and 99% (Table 3).

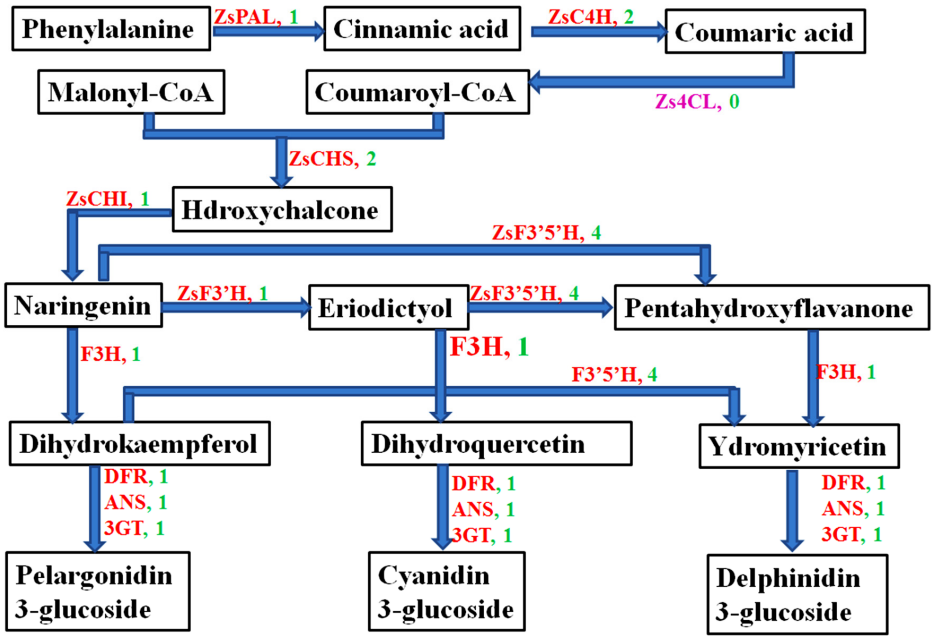

Figure 3. Anthocyanin metabolic pathway and anthocyanin-related structure gene number of *Z. striolatum*. PAL: Phenylalanine ammonia-lyase; C4H: Cinnamate 4-hydroxylase; 4CL: 4-coumarate-CoA ligase; CHS: Chalcone synthesis; CHI: Chalcone isomerase; F3H: Flavanone-3 hydroxylase; F3′H: Flavonoid 3′-hydroxylase; F3′5′H: Flavonoid-3′,5′-hydroxylase; DFR: Dihydroflavonol 4-reductase; ANS: Anthocyanidin synthase; 3GT: UDP-flavonoid 3-*O*-glucosyltransferase. The numbers of genes are marked in green.

Table 3. The information on anthocyanin biosynthesis genes in *Z. striolatum*.

No	Gene Name	Transcriptome Number	Length of ORF (bp)	Length of Amino Acid (aa)	Complete or Incomplete Sequence	NCBI Accession of *Z. officinale*	Length of *Z. officinale* Amino Acid (aa)	Query Cover (%)	E-Value
1	*ZsPAL*	Unigene7157	2163	720	Complete	XP_042378359.1	719	99	0
2	*ZsC4H-1*	Unigene8556	1512	503	Complete	XP_042449483.1	503	96	0
3	*ZsC4H-2*	Unigene40519	1512	503	Complete	XP_042465304.1	503	99	0
4	*ZsCHS-1*	Unigene17217	1188	395	Complete	XP_042470361.1	395	99	0
5	*ZsCHS-2*	Unigene18623	1176	391	Complete	XP_042434725.1	391	99	0
6	*ZsCHI*	Unigene3000	642	213	Complete	XP_042397410.1	213	99	2×10^{-131}
7	*ZsF3H*	Unigene17179	1164	387	Complete	XP_042448017.1	376	94	0
8	*ZsF3′H*	DN165_c2_g1	1560	519	Complete	XP_042383089.1	519	96	0
9	*ZsF3′5′H-1*	Unigene14062	1536	511	Complete	XP_042414732.1	513	99	0
10	*ZsF3′5′H-2*	Unigene14166	1536	511	Complete	XP_042431580.1	511	99	0
11	*ZsF3′5′H-3*	DN4439_c0_g1	1542	513	Complete	XP_042381450.1	513	88	0
12	*ZsF3′5′H-4*	Unigene13527	1536	511	Complete	XP_042399460.1	515	99	0
13	*ZsDFR*	DN13806_c2_g1	1077	358	Complete	XP_042421830.1	357	99	0
14	*ZsANS*	Unigene16060	1098	365	Complete	XP_042431763.1	365	95	0
15	*Zs3GT*	Unigene13244	1419	472	Complete	XP_042420251.1	472	99	0

3.4. Expression Level of Anthocyanin-Related Genes in Three Planting Modes of *Z. striolatum*

We detected the gene expression levels of anthocyanin-related genes under three planting modes of *Z. striolatum* by qPCR. The results indicated that the expression level of anthocyanin-related genes was significantly different in three planting modes of *Z. striolatum*. The anthocyanin-related genes were expressed in three planting modes. The expression levels of *ZsC4H-2* and *ZsDFR* genes were nearly 0 in SP, and the expression levels were the highest in ZP. The expression levels of *ZsPAL*, *ZsF3′5′H-2*, *ZsF3′5′H-4*, and *Zs3GT* genes in SP were significantly higher than those in ZP and CK. The expression levels of *ZsC4H-1*, *ZsC4H-2*, *ZsCHS-2*, *ZsCHI*, *ZsF3H*, *ZsF3′H*, *ZsDFR*, *ZsF3′5′H-3*, and *ZsANS* genes in ZP were significantly higher than those in the two other planting modes of *Z. striolatum*. Only the expression level of the *ZsF3′5′H-3* gene was significantly higher than that in ZP and SP. The expression level of the *ZsCHS-1* gene in CK and SP was basically the same, and the expression levels of both genes were significantly higher than that in ZP (Figure 4).

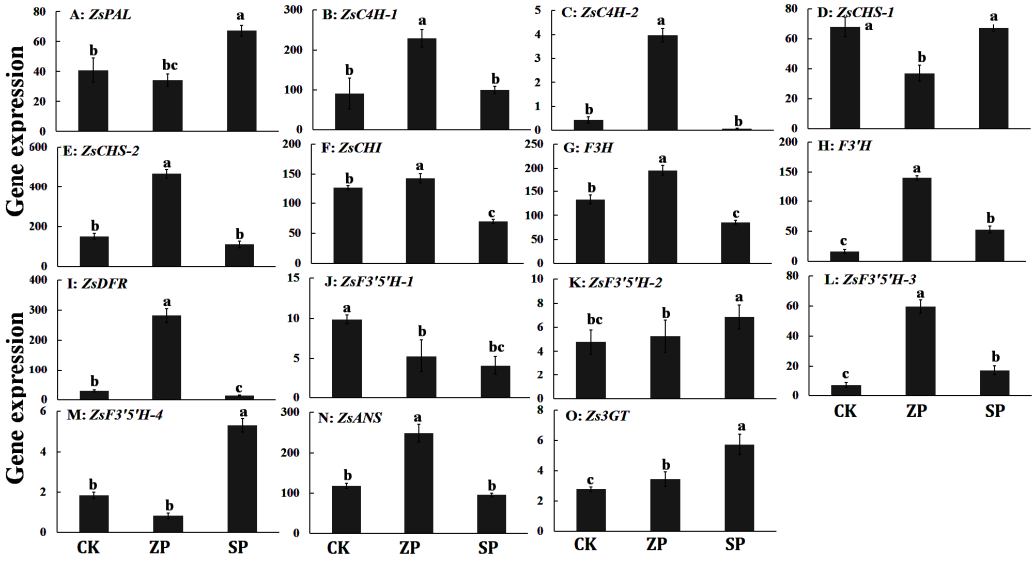

Figure 4. The expression level of anthocyanin-related genes of *Z. striolatum* in three planting modes. Different lowercase letters indicate the significance of the difference ($p < 0.05$).

3.5. Correlation Analysis Anthocyanin of Content and Expression Levels of Anthocyanin-Synthesis-Related Genes

The relationship between anthocyanin content and the expression level of anthocyanin-synthesis-related genes was further defined through correlation analysis. The correlation results (Table S3) showed that the total anthocyanin content was significantly positively correlated with the expression levels of *ZsC4H-1*, *ZsC4H-2*, *ZsCHS-2*, *ZsCHI*, *ZsF3H*, *ZsDFR*, *ZsF3′H*, *ZsF3′5′H-3*, and *ZsANS* genes. Meanwhile, it was significantly negatively correlated with the expression levels of *ZsPAL*, *ZsCHS-1*, and *ZsF3′5′H-4* genes. The total anthocyanin content was positively correlated with the expression level of the *ZsF3′5′H-1* gene, while it was negatively correlated with the expression level of the *ZsF3′5′H-2* gene. Petunidin-3-*O*-(6-*O*-p-coumaroyl)-glucoside, delphinidin-3-*O*-(6-*O*-malonyl-beta-D-glucoside), delphinidin-3-*O*-(6-*O*-malonyl)-glucoside-3′-glucoside, malvidin-3-*O*-(6″-*O*-acetyl) glucoside, malvidin-3-*O*-rhamnoside, cyanidin-3-*O*-rhamnoside, cyanidin-rutinoside-rhamnoside, pelargonidin-3-*O*-(6″-*O*-acetyl) galactoside, and pelargonidin-3-*O*-galactoside showed an opposite relationship to the correlation between total anthocyanin content and the expression levels of anthocyanin structure genes, while the remaining anthocyanin monomer remained consistent.

4. Discussion

We selected the purple *Z. striolatum* with the largest cultivation area in Guizhou Province as the experimental material to explore the best planting method for improving the yield and quality of *Z. striolatum*. Moreover, three planting methods—CK, ZP, and SP—were adopted. The results showed significant differences in yield and anthocyanin accumulation of *Z. striolatum* among the three planting patterns. Analysis of the three aspects of flower bud germination, commercial flower bud size, and anthocyanin accumulation of *Z. striolatum* indicated that the germination rate of *Z. striolatum* flower buds in the root was high, the commodity flower buds was large, and the anthocyanin accumulation was obvious, which improved the yield and anthocyanin accumulation of *Z. striolatum*. This phenomenon was directly related to light. On the one hand, the planting mode of SP can increase canopy photosynthesis [35,36], and the *Z. striolatum* flower buds prefer to live in shady and cool environments [37]. On the other hand, anthocyanins can accelerate the degradation of anthocyanins in light [38,39]. In this study, maize could better shade for the *Z. striolatum* growth and increase its flower bud yield and anthocyanins content, indicating that ZP can provide a cool and shaded light environment for the growth of *Z. striolatum*.

The composition and content of anthocyanin are the main factors affecting the coloration of *Z. striolatum* flower buds. In this study, 48 anthocyanins were identified in the *Z. striolatum* flower buds by the combination of targeted metabolomics for the first time. A total of 17 cyanidins were detected in the *Z. striolatum* flower buds, among which the cyanidin-3-*O*-glucoside content was the highest, which may be the main pigment type in Z. striolatum flower buds. Cyanidin was the main pigment that leads to purple color in many horticultural crops [40,41]. Notably, 7 peonidins were detected in CK and ZP, while only 2 peonidins were detected in SP. The result indicated that the planting mode of SP was detrimental to the synthesis and accumulation of peonidin, which may be related to the nitrogen fixation of leguminous crops. Nitrogen is an important regulator of anthocyanin synthesis and accumulation in plants. In general, plants can promote anthocyanin synthesis under low nitrogen conditions, while they inhibit anthocyanin synthesis and accumulation under high nitrogen conditions [42–44].

The biosynthesis pathway for anthocyanins has been studied in various model crops, such as *Arabidopsis thaliana*, and was highly conserved in many plants [45]. *ZsCHS*, *ZsCHI*, *ZsF3H*, *ZsF3′H*, *ZsF3′5′H*, *ZsDFR*, *ZsANS*, and *Zs3GT* genes were the key genes affecting the coloration of *Z. striolatum* flower buds. These genes were significantly upregulated in *Z. striolatum* flower buds, which promote anthocyanin biosynthesis. *F3H* was an important branch point in the anthocyanin biosynthesis pathway, and the *ZsF3H* gene was significantly related to the total anthocyanin content of *Z. striolatum* flower buds. Thus, it

may be one of the key genes leading to the anthocyanin difference of *Z. striolatum* flower buds [46]. *DFR*, *ANS*, and *3GT* genes were downstream genes of the biosynthesis pathway for anthocyanins. Flavonols were catalyzed to colorless anthocyanin by dihydroflavonol-4-reductase, which was further catalyzed to form the colored anthocyanins by anthocyanidin synthase [47,48]. The expression levels of *ZsDFR* and *ZsANS* genes in ZP were significantly higher than those in CK and SP, which was consistent with the anthocyanins content in the three planting modes. Colored anthocyanins were catalyzed to stabilize anthocyanins using UDP-flavonoid 3-*O*-glucosyItransferase [49]. The results revealed that the expression level of the *Zs3GT* gene was significantly higher in ZP than in the two other planting modes, which indicated that the anthocyanin of *Z. striolatum* flower buds was more stable and difficult to degrade. Studies have found that *F3′H* and *F3′5′H* genes are key genes in the biosynthesis pathways of red and blue anthocyanins, respectively [50]. Blue anthocyanins were also detected in *Z. striolatum* flower buds in the present study. Therefore, *Z. striolatum* may contain abundant modified gene resources for breeding red and blue *Z. striolatum* flower buds.

In this study, we identified 15 structural genes from the transcriptome database of *Z. striolatum* according to the biosynthesis pathway for anthocyanins. Intriguingly, the *Zs4CL* gene was not aligned. We also found similar situations in *Dendrobium* [51], red okra [52], and *Cymbidium orchid* [53]. We speculate that the biosynthesis pathway for anthocyanins in *Z. striolatum* flower buds may be the same as most crops and affected by light-induced [54–56]. Therefore, the biosynthesis pathway for anthocyanins in *Z. striolatum* flower buds still needs to be further improved.

5. Conclusions

We adopted three planting modes of *Z. striolatum*, including *Z. striolatum* monoculture (CK), intercropping with maize (ZP), and intercropping with soybean (SP). The results showed that the commodity flower buds were large, and the anthocyanin content was high in the planting mode of ZP, which could effectively improve the yield and quality of *Z. striolatum* flower buds, the content of cyanidin-3-*O*-glucoside was the highest, and the main type of anthocyanins in *Z. striolatum* flower buds. These findings provide valuable information for the research of the planting model of *Z. striolatum* flower buds.

Supplementary Materials: The following supporting information can be downloaded at: https://www.mdpi.com/article/10.3390/agronomy14071414/s1, Table S1. The sequence information of genes involved in the anthocyanidin biosynthesis; Table S2. Primers used in this study; Table S3. Correlation of anthocyanin contents and anthocyanin-related genes relative expression levels in three planting modes.

Author Contributions: D.Z., T.W. and G.T. conceived and designed the experiment; D.Z. analyzed the data; D.Z., T.W., Q.Z. and G.T. contributed reagents/materials/analysis tools; D.Z. performed the experiments; D.Z. and Q.Z. wrote the paper: D.Z. and G.T. revised the paper. All authors have read and agreed to the published version of the manuscript.

Funding: The research was supported by the Qiankehe Service Enterprise [2022] 005, Qianke Hezhong Land Diversion [2023] 033), Construction of Modern Agricultural Industry Technology System in Guizhou Province Vegetable System Project (GZCYTX2024-0101), and Guizhou Province Plateau Characteristic Vegetable Industry Technology System (GZMARS).

Data Availability Statement: The original contributions presented in the study are included in the article; further inquiries can be directed to the corresponding author.

Conflicts of Interest: The authors declare no conflict of interest.

References

1. Huang, Z.B.; Xie, L.N.; Wang, H.W.; Zhong, J.B.; Li, Y.C.; Liu, J.L.; Ou, Z.R.; Liang, X.; Li, Y.S.; Huang, H.Y.; et al. Geographic distribution and impacts of climate change on the suitable habitats of *Zingiber* species in China. *Ind. Crops Prod.* **2019**, *138*, e111429. [CrossRef]
2. Tian, S.M.; Jiang, D.Z.; Wan, Y.P.; Wang, X.; Liao, Q.H.; Li, Q.; Li, H.L.; Liao, L.Z. The complete chloroplast genome of *Zingiber striolatum* Diels (Zingiberaceae). *Mitochondrial DNA Part B Resour.* **2023**, *8*, 48–51. [CrossRef]
3. Yang, J.; Li, Y.C.; He, Y.X.; He, H.Y.; Chen, X.Q.; Liu, T.F.; Zhu, B. Wild vs. cultivated *Zingiber striolatum* Diels: Nutritional and biological activity differences. *Plants* **2023**, *12*, e2180. [CrossRef]
4. Huang, Z.B.; Xie, L.N.; Xu, Y.Y.; Zhao, K.; Li, X.T.; Zhong, J.B.; Lu, Y.J.; Xu, X.T.; Goodin, S.; Zhang, K.; et al. Essential oils from *Zingiber striolatum* Diels attenuate inflammatory response and oxidative stress through regulation of MAPK and NF-κB signaling pathways. *Antioxidants* **2021**, *10*, e2019. [CrossRef]
5. Chen, T.; Cai, J.; Ni, J.; Yang, F. An UPLC-MS/MS application to investigate chemical compositions in the ethanol extract with hypoglycemic activity from *Zingiber striolatum* Diels. *J. Chin. Pharm. Sci.* **2016**, *25*, 116–121. [CrossRef]
6. Kim, H.W.; Murakami, A.; Abe, M.; Ozawa, Y.; Morimitsu, Y.; Williams, M.V.; Ohigashi, H. Suppressive effects of mioga ginger and ginger constituents on reactive oxygen and nitrogen species generation, and the expression of inducible pro-inflammatory genes in macrophages. *Antioxid. Redox Signal.* **2005**, *7*, 1621–1629. [CrossRef]
7. Tian, M.; Liu, T.; Wu, X.; Hong, Y.; Zhou, Y. Chemical composition, antioxidant, antimicrobial and anticancer activities of the essential oil from the rhizomes of *Zingiber striolatum* Diels. *Nat. Prod. Res.* **2020**, *34*, 2621–2625. [CrossRef]
8. Chaves-Silva, S.; dos Santos, A.L.; Chalfun-Junior, A.; Zhao, J.; Peres, L.E.P.; Benedito, V.A. Understanding the genetic regulation of anthocyanin biosynthesis in plants—Tools for breeding purple varieties of fruits and vegetables. *Phytochem.* **2018**, *153*, 11–27. [CrossRef]
9. Sharma, H.; Sharma, P.; Kumar, A.; Chawla, N.; Dhatt, A.S. Multifaceted regulation of anthocyanin biosynthesis in plants: A comprehensive review. *J. Plant Growth Regul.* **2024**, *12*, 1–15. [CrossRef]
10. Ren, Y.; Huang, Z.Q.; Jiang, H.; Wang, Z.; Wu, F.S.; Xiong, Y.F.; Yao, J.L. A heat stress responsive NAC transcription factor heterodimer plays key roles in rice grain filling. *J. Exp. Bot.* **2021**, *72*, 2947–2964. [CrossRef]
11. Cui, L.G.; Shan, J.X.; Shi, M.; Gao, J.P.; Lin, H.X. The miR156-SPL9-DFR pathway coordinates the relationship between development and abiotic stress tolerance in plants. *Plant J.* **2014**, *80*, 1108–1117. [CrossRef]
12. Hatier, J.H.B.; Clearwater, M.J.; Gould, K.S. The functional significance of black-pigmented leaves: Photosynthesis, photoprotection and productivity in *Ophiopogon planiscapus* 'Nigrescens'. *PLoS ONE* **2013**, *8*, e67850. [CrossRef]
13. Qi, F.T.; Liu, Y.T.; Luo, Y.L.; Cui, Y.M.; Lu, C.F.; Li, H.; Huang, H.; Dai, S.L. Functional analysis of the ScAG and SCAGL11 MADS-box transcription factors for anthocyanin biosynthesis and bicolour pattern formation in *Senecio cruentus* ray florets. *Hortic. Res.* **2022**, *9*, uhac071. [CrossRef]
14. Baumann, K.; Perez-Rodriguez, M.; Bradley, D.; Venail, J.; Bailey, P.; Jin, H.; Koes, R.; Roberts, K.; Martin, C. Control of cell and petal morphogenesis by R2R3 MYB transcription factors. *Development* **2007**, *134*, 1691–1701. [CrossRef]
15. Shen, H.; Han, J.; Liu, C.L.; Cao, F.; Huang, Y.J. Grape seed proanthocyanidins exert a radioprotective effect on the testes and intestines through antioxidant effects and inhibition of MAPK signal pathways. *Front. Med.* **2022**, *8*, e836528. [CrossRef]
16. Zhou, P.Y.; Zhang, L.M.; Li, W.; Zhang, S.T.; Luo, L.X.; Wang, J.; Sun, B.S. In vitro evaluation of the anti-digestion and antioxidant effects of grape seed procyanidins according to their degrees of polymerization. *J. Funct. Foods* **2018**, *49*, 85–95. [CrossRef]
17. Le, D.H.; Nishimura, K.; Takenaka, Y.; Mizushina, Y.; Tanahashi, T. Polyprenylated benzoylphloroglucinols with DNA polymerase inhibitory activity from the fruits of *Garcinia schomburgkiana*. *J. Nat. Prod.* **2016**, *79*, 1798–1807. [CrossRef]
18. Yamagishi, M. High temperature enhances anthocyanin coloration in *Asiatic* hybrid lily flowers via upregulation of the MYB12 positive regulator. *Hortic. Plant J.* **2022**, *8*, 769–776. [CrossRef]
19. Brugliera, F.; Tao, G.Q.; Tems, U.; Kalc, G.; Mouradova, E.; Price, K.; Stevenson, K.; Nakamura, N.; Stacey, I.; Katsumoto, Y.; et al. Violet/blue chrysanthemums: Metabolic engineering of the anthocyanin biosynthetic pathway results in novel petal colors. *Plant Cell Physiol.* **2013**, *54*, 1696–1710. [CrossRef]
20. Feng, X.K.; Gao, G.; Yu, C.M.; Zhu, A.G.; Chen, J.K.; Chen, K.M.; Wang, X.F.; Abubakar, A.S.; Chen, P. Transcriptome and metabolome analysis reveals anthocyanin biosynthesis pathway associated with ramie (*Boehmeria nivea* (L.) Gaud. leaf color formation. *BMC Genom.* **2021**, *22*, e684. [CrossRef]
21. Zhang, Y.J.; Chu, G.H.; Hu, Z.L.; Gao, Q.; Cui, B.L.; Tian, S.B.; Wang, B.; Chen, G.P. Genetically engineered anthocyanin pathway for high health-promoting pigment production in eggplant. *Mol. Breed.* **2016**, *36*, 54. [CrossRef]
22. Qi, X.W.; Shuai, Q.; Chen, H.; Fan, L.; Zeng, Q.W.; He, N.J. Cloning and expression analyses of the anthocyanin biosynthetic genes in mulberry plants. *Mol. Genet. Genom.* **2014**, *289*, 783–793. [CrossRef]
23. Sunil, L.; Shetty, N.P. Biosynthesis and regulation of anthocyanin pathway genes. *Appl. Microbiol. Biotechnol.* **2022**, *106*, 1783–1798. [CrossRef]
24. Bloor, S.J.; Abrahams, S. The structure of the major anthocyanin in *Arabidopsis thaliana*. *Phytochemistry* **2002**, *59*, 343–346. [CrossRef]
25. Xu, Z.S.; Huang, Y.; Wang, F.; Song, X.; Wang, G.L.; Xiong, A.S. Transcript profiling of structural genes involved in cyanidin-based anthocyanin biosynthesis between purple and non-purple carrot (*Daucus carota* L.) cultivars reveals distinct patterns. *BMC Plant Biol.* **2014**, *14*, e262. [CrossRef]

26. Liu, Y.J.; Li, M.; Li, T.T.; Chen, Y.J.; Zhang, L.J.; Zhao, G.F.; Zhuang, J.H.; Zhao, W.Y.; Gao, L.P.; Xia, T. Airborne fungus-induced biosynthesis of anthocyanins in *Arabidopsis thaliana* via jasmonic acid and salicylic acid signaling. *Plant Sci.* **2020**, *300*, e110635. [CrossRef]
27. Zhang, Y.; Chen, C.Q.; Cui, Y.L.; Du, Q.S.; Tang, W.J.; Yang, W.L.; Kou, G.Q.; Tang, W.J.; Chen, H.X.; Gong, R.G. Potential regulatory genes of light induced anthocyanin accumulation in sweet cherry identified by combining transcriptome and metabolome analysis. *Front. Plant Sci.* **2023**, *14*, e1238624. [CrossRef]
28. Jiao, Y.; Ma, R.J.; Shen, Z.J.; Yan, J.; Yu, M.L. Gene regulation of anthocyanin biosynthesis in two blood-flesh peach (*Prunus persica* (L.) Batsch) cultivars during fruit development. *J. Zhejiang Univ. Sci. B* **2014**, *15*, 809–819. [CrossRef]
29. Wu, Y.Q.; Hao, Z.J.; Tang, Y.H.; Zhao, D.Q. Anthocyanin accumulation and differential expression of the biosynthetic genes result in a discrepancy in the red color of herbaceous peony (*Paeonia lactiflora* Pall.) flowers. *Horticulturae* **2022**, *8*, e349. [CrossRef]
30. Tanaka, Y.; Sasaki, N.; Ohmiya, A. Biosynthesis of plant pigments: Anthocyanins, betalains and and carotenoids. *Plant J.* **2008**, *54*, 733–749. [CrossRef]
31. Jin, X.H.; Huang, H.; Wang, L.; Sun, Y.; Dai, S.L. Transcriptomics and metabolite analysis reveals the molecular mechanism of anthocyanin biosynthesis branch pathway in different *Senecio cruentus* cultivars. *Front. Plant Sci.* **2016**, *7*, e1307. [CrossRef] [PubMed]
32. Chai, Z.; Herrera-Balandrano, D.D.; Yu, H.; Beta, T.; Zeng, Q.L.; Zhang, X.X.; Tian, L.L.; Niu, L.Y.; Huang, W.Y. A comparative analysis on the anthocyanin composition of 74 blueberry cultivars from China. *J. Food Compos. Anal.* **2021**, *102*, e104051. [CrossRef]
33. Katsumoto, Y.; Fukuchi-mizutani, M.; Fukui, Y.; Brugliera, F.; Holton, T.; Karan, M.; Nakamura, N.; Yonekura-Sakakibara, K.; Togami, J.; Pigeaire, A.; et al. Engineering of the rose flavonoid biosynthetic pathway successfully generated blue-hued flowers accumulating delphinidin. *Plant Cell Physiol.* **2007**, *48*, e1589. [CrossRef]
34. Noda, N. Recent advances in the research and development of blue flowers. *Breed. Sci.* **2018**, *68*, 79–87. [CrossRef]
35. Wang, Q.S.; Sun, D.B.; Hao, H.; Zhao, X.J.; Hao, W.P.; Liu, Q. Photosynthetically active radiation determining yields for an intercrop of maize with cabbage. *Eur. J. Agron.* **2015**, *69*, 32–40. [CrossRef]
36. Chi, B.J.; Liu, J.; Dai, J.L.; Li, Z.H.; Zhang, D.M.; Xu, S.Z.; Nie, J.J.; Wan, S.M.; Li, C.D.; Dong, H.Z. Alternate intercropping of cotton and peanut increases productivity by increasing canopy photosynthesis and nutrient uptake under the influence of rhizobacteria. *Field Crop. Res.* **2023**, *302*, e109059. [CrossRef]
37. Deng, K.P.; Deng, R.J.; Fan, J.X.; Chen, E.F. Transcriptome analysis and development of simple sequence repeat (SSR) markers in *Zingiber striolatum* Diels. *Physiol. Mol. Biol. Plants* **2018**, *24*, 125–134. [CrossRef]
38. Cai, D.B.; Li, X.S.; Chen, J.L.; Jiang, X.W.; Ma, X.Q.; Sun, J.X.; Tian, L.M.; Vidyarthi, S.K.; Xu, J.W.; Pan, Z.L.; et al. A comprehensive review on innovative and advanced stabilization approaches of anthocyanin by modifying structure and controling environmental factors. *Food Chem.* **2022**, *366*, e130611. [CrossRef]
39. Jin, W.P.; Xiang, L.; Peng, D.F.; Liu, G.; He, J.R.; Cheng, S.Y.; Li, B.; Huang, Q.R. Study on the coupling progress of thermo-induced anthocyanins degradation and polysaccharides gelation. *Food Hydrocoll.* **2020**, *105*, e105822. [CrossRef]
40. Liu, Y.; Tikunov, Y.; Schouten, R.E.; Marcelis, L.F.M.; Visser, R.G.F.; Bovy, A. Anthocyanin biosynthesis and degradation mechanisms in Solanaceous vegetables: A review. *Front. Chem.* **2018**, *6*, e52. [CrossRef] [PubMed]
41. Wang, N.H.; Dai, M.Y.; Zheng, G.; Chang, P.J.; Xuan, L.J.; Liu, Z.G.; Wang, Y.L.; Cheng, S.Y.; Wang, Z.; Wang, H.; et al. Flavonold components and gene expression analysis reveal flower pigmentation difference between *Magnolia biondi* and its variety *M. biondi* var. purpurascens. *Trees* **2022**, *36*, 583–591. [CrossRef]
42. Rubin, G.; Tohge, T.; Matsuda, F.; Saito, K.; Scheible, W.R. Members of the LBD family of transcription factors repress anthocyanin synthesis and affect additional nitrogen responses in *Arabidopsis*. *Plant Cell* **2009**, *21*, 3567–3584. [CrossRef]
43. Zhou, L.L.; Shi, M.Z.; Xie, D.Y. Regulation of anthocyanin biosynthesis by nitrogen in TTG1-GL3/TT8-PAP1- programmed red cells of *Arabidopsis thaliana*. *Planta* **2012**, *236*, 825–837. [CrossRef]
44. Wang, J.; Wang, Y.; Yang, J.; Ma, C.L.; Zhang, Y.; Ge, T.; Qi, Z.; Kang, Y. *Arabidopsis* ROOT HAIR DEFECTIVE3 is involved in nitrogen starvation-induced anthocyanin accumulation. *J. Integr. Plant Biol.* **2015**, *57*, 708–721. [CrossRef]
45. Grützner, R.; König, K.; Horn, C.; Engler, C.; Laub, A.; Vogt, T.; Marillonnet, S. A transient expression tool box for anthocyanin biosynthesis in *Nicotiana benthamiana*. *Plant Biotechnol. J.* **2023**, *143*, 1238–1250. [CrossRef]
46. Song, B.; Xu, H.; Chen, L.Z.; Fan, X.X.; Jing, Z.G.; Chen, S.; Xu, Z.G. Study of the relationship between leaf color formation and anthocyanin metabolism among different purple pakchoi lines. *Molecules* **2020**, *25*, e4809. [CrossRef]
47. Feng, X.; Zhang, Y.T.; Wang, H.; Tian, Z.D.; Xin, S.Y.; Zhu, P.F. The dihydroflavonol 4-reductase BoDFR1 drives anthocyanin accumulation in pink-leaved ornamental kale. *Theor. Appl. Genet.* **2021**, *134*, 159–169. [CrossRef]
48. Jaakola, L. New insights into the regulation of anthocyanin biosynthesis in fruits. *Trends Plant Sci.* **2013**, *18*, 477–483. [CrossRef]
49. Matsuba, Y.; Sasaki, N.; Tera, M.; Okamura, M.; Abe, Y.; Okamoto, E.; Nakamura, H.; Funabashi, H.; Takatsu, M.; Saito, M.; et al. A novel glucosylation reaction on anthocyanin catalyzed by acyl-glucose-dependent glucosyltransferase in the petals of carnation and delphinium. *Plant Cell* **2010**, *22*, 3374–3389. [CrossRef]
50. Huang, H.; Hu, K.; Han, K.T.; Xiang, Q.Y.; Dai, S.L. Flower colour modification of chrysanthemum by suppression of *F3′H* and overexpression of the exogenous *Senecio cruentus F3′5′H* gene. *PLoS ONE* **2013**, *8*, e74395. [CrossRef]
51. Wu, M.Q.; Liao, Y.; Lu, S.J.; Yin, H.T.; Yu, W.G.; Li, C.H. Metabolomics analysis of anthocyanin in different flower colors of phalaenopsis-type *Dendrobium* (in Chinese with abstract). *Chin. J. Trop. Crops* **2023**, *44*, 2167–2178. [CrossRef]

52. Wang, J.Q.; Zhang, Y.H.; Yi, W.Y.; Gong, Z.G.; Xu, H.B.; Li, Y.Y. Study on genes related to anthocyanin biosynthesis at the color turning stages in red okra fruit based on transcriptome sequencing. *N. Hortic.* **2022**, *14*, 9–16.
53. Wang, L.; Albert, N.W.; Zhang, H.B.; Arathoon, S.; Boase, M.R.; Ngo, H.; Schwinn, K.E.; Davies, K.M.; Lewis, D.H. Temporal and spatial regulation of anthocyanin biosynthesis provide diverse flower colour intensities and patterning in *Cymbidium* orchid. *Planta* **2014**, *240*, 983–1002. [CrossRef] [PubMed]
54. Zhou, Y.; Wu, W.S.; Sun, Y.; Shen, Y.Y.; Mao, L.Z.; Dai, Y.H.; Yang, B.Z.; Liu, Z.B. Integrated transcriptome and metabolome analysis reveals anthocyanin biosynthesis mechanisms in pepper (*Capsicum annuum* L.) leaves under continuous blue light irradiation. *BMC Plant Biol.* **2024**, *24*, e10. [CrossRef] [PubMed]
55. Fan, D.; Wang, X.; Liu, T.; Liu, H.; Peng, Y.; Tang, X.; Ye, X.; Sun, K.; Yue, Y.; Xu, D.; et al. Epigenetic regulation of high light-induced anthocyanin biosynthesis by histone demethylase IBM1 in *Arabidopsis*. *New Phytol.* **2024**, *242*, 2570–2585. [CrossRef]
56. Zhao, Q.; Zhong, X.L.; Cai, X.; Zhu, S.H.; Meng, P.H.; Zhang, J.; Tan, G.F. Comparative physiological analysis of lignification, anthocyanin metabolism and correlated gene expression in red *Toona sinensis* buds during cold storage. *Agronomy* **2023**, *13*, e119. [CrossRef]